J of Astronaut Sci (2013) 60:258–277
DOI 10.1007/s40295-015-0048-y

# Prospects of Relative Attitude Control Using Coulomb Actuation

**Hanspeter Schaub**[1,2] · **Daan Stevenson**[1,2]

Published online: 15 July 2015
© American Astronautical Society 2015

**Abstract** The relative attitude is studied between two charge controlled spacecraft being held at a fixed separation distance. While one body has a spherical shape, the 2nd body is assumed to be non-spherical and tumbling. The attitude control goal is to arrest the rotation of the 2nd body. While prior work has identified the existence of torques between charged bodies, this is the first analytical study on a charged feedback attitude control. Using the recently developed multi-sphere method to provide a simplified electrostatic force and torque model between non-spherical shapes, Lyapunov theory is used to develop a stabilizing attitude control using spacecraft potential as the control variable. Zero and non-zero equilibrium potentials are considered, with the later suitable for the electrostatic tug concept. With a pulling configuration, the cylinder will come to rest with the long axis aligned with the inter-vehicle axis in a stable configuration. For a pusher, the cylinder will settle 90 degrees rotated from this axis. Numerical simulations illustrate the control performance.

**Keywords** Coulomb actuation · Attitude control · Touchless detumbling

✉ Hanspeter Schaub
hanspeter.schaub@colorado.edu

[1] Department of Aerospace Engineering Sciences, University of Colorado, Boulder, CO 431 UCB, USA

[2] Colorado Center for Astrodynamics Research, Boulder, CO 80309-0431, USA

## Introduction

Electrostatic actuation in space has been proposed as early as 1966 by Cover et. al. in Reference [1]. Active charging is proposed to actuate a membrane attached to a solid outer structure of a geostationary satellite. The Geosynchronous Orbit (GEO) region is shown to require very low current emission to maintain a non-equilibrium potential on a space object, yielding Watt-levels of power requirements. The required mass emission for this electrostatic or Coulomb actuation is so low, this mode of actuation is often referred to as essentially propellantless. Later, in 2003, Reference [2] reiterates the virtues of Coulomb actuation at GEO, and studies the prospects of using Coulomb forces to control the relative motion of free-flying spacecraft dozens of meters apart. Novel charged astrodynamics equilibria are identified illustrating the new types of close proximity flying missions that are enabled through this low-propellant relative motion control method.

However, the fuel-efficiency comes at a cost of complex, strongly-coupled nonlinear relative differential equations of motion, yielding a non-affine control problem for the general $N$-cluster scenario. Coulomb formation flying (CFF) dynamics and control has been studied in numerous publications, but much work remains to be done to fully understand the complex relative motion behaviors, and identity promising mission scenarios. Analytical solutions for fixed formation shape charged equilibria are discussed in References [3–5], while feedback control on 2- and 3-craft formations are discussed in References [6–8]. Hybrid relative motion control employing both inertial thrusters and electrostatic actuation allows for more general relative motion control where the electrostatics don't provide full controllability [9–13]. Other charged astrodynamics research has focused on charging spacecraft to large potentials to exploit the interaction with the planet's magnetic and generate Lorentz-Augmented Orbits (LAO) [14–16].

Most prior studies have focused on studying the electrostatic forces and the relative translational motion that results. Flying two charged spacecraft dozens of meters apart can yield electrostatic torques as well as forces. Reference [2] uses the NASCAP software (NASA/Air Force Spacecraft Charging Analysis Program) to model the expected force and torque levels for a range of spacecraft potentials at GEO conditions. The torques are identified as a significant influence if the craft are flying very close, on the order of 1-3 craft radii, but no dynamic analysis is performed. The prospects of using electrostatic torques for attitude control is mentioned in Reference [17], but no attitude dynamics are simulated. A reason for the lack of charged relative attitude dynamics studies is the complexity in modeling the electrostatic torques. Because the torques are only significant at very close separation distances of a few craft radii, common simplifying assumptions, such as the vehicle capacitance being evaluated using isolated body models, are no longer valid. The presence of another charged body impacts the capacitance of each vehicle, as has been experimentally demonstrated [18, 19]. While it is possible to use numerical finite element solvers to determine the electrostatic fields about a cluster of general shapes, it can take minutes and longer to evaluate a single force solution. This is not suitable for

numerical simulations of the attitude dynamics where a single test run can require 10,000's of force evaluations.

A recently proposed electrostatic force modeling technique, called the Multi-Sphere Method (MSM) is able to provide a reduced order model suitable for faster-than-realtime dynamic simulations [20, 21]. Both bodies are assumed to have a conducting outer surface, such that constant surface potential is maintained with active charge emission. The general shape is discretized through a series of spheres, all held at the same potential of the spacecraft. Using the position dependent capacitance model of a series of spheres [22, 23], the electrostatic force evaluation is reduced to a linear algebra problem that can be solved in a fraction of a second.

The MSM is used in this study to investigate potential feedback control strategies to arrest the motion of a tumbling object. This is the first study where the charged relative motion dynamics are consider and simulated. One motivation of this work is a recently introduced electrostatic tug concept where charge transfer is employed to create an electrostatic force with a space tug to move large geostationary space debris [24]. Here active inertial control is applied to maintain a fixed separation distance while engaging the electrostatic tractor [25]. If the debris rotational momentum could be arrested without physical contact, it would make any docking mission with space debris much simpler. Other applications include performing general CFF orbit corrections where a sub-set of the cluster nodes have inertial thrusting capabilities, and the remaining objects are electrostatically tugged [25].

If the net charge and charge distribution on each body were fixed, then the electrostatic attitude problem would be similar mathematically to the gravity gradient torque attitude problem of orbiting spacecraft. Unlike the small second body assumption made when computing the gravity gradient equilibria of a spacecraft, the electrostatic relative equilibria between two charged bodies makes no such relative size assumption. Further, because with active charging the potential is controlled, the charge distribution for closely neighboring objects varies as a function of the relative position and orientation of the objects [19, 22, 23].

The scope of this work considers only one-dimensional rotational motion, and assumes the non-tumbling vehicle (i.e. tug) is spherical in shape. This initial study considers the non-spherical, tumbling space body to be cylindrical. Further, the important issue of robustness is left to future work where experimental demonstrations of these attitude control solutions are being developed. Because the separation distances are only dozens of meters, and the GEO Debye length is around 200 meters, [26] the space plasma will have a negligible impact on the electrostatic actuation. Thus, vacuum conditions are assumed for this paper. The space weather or neighboring plasma will have an impact on the required electrical power requirements. As discussed in Reference [1], these power requirements are very low around Watt-levels. The potential levels considered in this study range up to 20kV. This potential level has been observed to naturally occur at times in GEO [27]. As in prior Coulomb formation flying research, this work assumes a potential servo control is present which is able to create desired potential levels using charge emission. Thus for the

purposes of this study the vehicle potential is treated as the fundamental control variable.

For GEO space debris reorbiting to a disposal region, the cylinder shape is of interest as many old dual-spinner configurations and rocket bodies need to be moved outside the GEO zone. The only control used are the spacecraft potentials which are assumed to be of equal magnitude for each body. This assumption is the preferred potential arrangement for an electrostatic tug, and thus has great practical relevance. Of interest is wether the tumbling body be brought to rest, and are repulsive and attractive forces required? Further, if the nominal spacecraft potential is non-zero, as in the electrostatic tug scenario, to what attitudes will the tumbling body converge?

The paper is organized as follows. First, the multi-sphere method is reviewed, and a particular solution is provided for a representative cylindrical spacecraft body. A simplified electrostatic torque model is considered suitable for the feedback control development. The charged relative attitude orientations for a slender cylinder are discussed along with their stability. Finally, nonlinear control strategies are considered to detumble the second object while maintaining a fixed separation distance. Numerical simulations illustrate the closed loop performance.

## Multi-Sphere Method

In order to develop the stability arguments for the remote attitude control of spacecraft by charge transfer, the relative motion dynamics must be modeled. There is no simple analytic solution for the electrostatic interaction between charged conductors with generic geometries. Several options exist for the numerical modeling of spacecraft charging and interactions, including finite element methods, finite difference methods, boundary element methods, and Monte Carlo methods [28, 29]. Each of these approaches, however, are too computationally expensive to allow for faster-than-real-time simulations of the electrostatically induced relative motion dynamics.

Simpler methods such as the point charge approximation and finite sphere model that have been used for Coulomb charge control analysis in the past [19, 25, 30] are limited to line-of-site forces and incapable of predicting electrostatic torques. The recently developed Multi Sphere Model (MSM) [20] uses a set of conductive spheres throughout the geometry of a spacecraft to capture the 3D electrostatic effects. Specifically, this reference provides detailed analysis of the interaction between a charged cylinder and a sphere, and this system will be used to study the de-spin control concepts that are the basis of this manuscript. While it is possible to capture the induced charge effects that occur with very close proximity scenarios with a larger set of spheres distributed on the surface of the objects [21], the 3D effects that result in torques exerted on the cylinder at larger separation distances are sufficiently captured when three spheres are used in the cylinder model. While the voltage of the three spheres representing the cylinder are held at the same potential, the resulting approximated charge distribution will be non-homogeneous.

Figure 1 shows the cylinder-sphere system using a three sphere MSM to represent the cylinder. The defining system parameters are the separation distance $d$, the cylin-

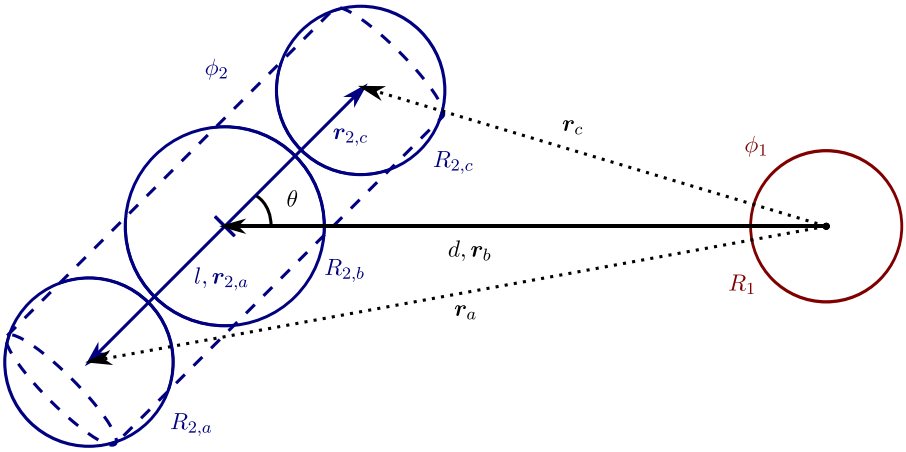


**Fig. 1** 3 sphere MSM for cylinder-sphere configuration

der orientation angle $\theta$, and the controlled voltages $\phi_1$ and $\phi_2$. The spheres in the cylinder are separated by $l$ while the remaining relative distances are:

$$r_a = \sqrt{l^2 + d^2 + 2ld\cos\theta} \tag{1}$$

$$r_b = d \tag{2}$$

$$r_c = \sqrt{l^2 + d^2 - 2ld\cos\theta} \tag{3}$$

Here $R_1$ is the radius of the spherical body on the right, while the cylindrical body is approximated through three spheres of radii $R_{2,a}$, $R_{2,b}$ and $R_{2,c}$.

The electrostatic forces are determined by the charges residing on each sphere. These result from the prescribed electric potentials, according to the self and mutual capacitance relationships in Eq. 4, where $k_c = 8.99 \times 10^9$ Nm$^2$/C$^2$ is Coulomb's constant [19, 22, 23, 31].

$$\phi_i = k_c \frac{q_i}{R_i} + \sum_{j=1, j\neq i}^{m} k_c \frac{q_j}{r_{i,j}} \tag{4}$$

Here $R_i$ are the sphere radii, $q_j$ are the charges on each sphere, and $r_{i,j}$ are the sphere to sphere separation distances. These relations can be combined for each sphere to obtain the matrix equation

$$\begin{bmatrix} \phi_1 \\ \phi_2 \\ \phi_2 \\ \phi_2 \end{bmatrix} = k_c \underbrace{\begin{bmatrix} 1/R_1 & 1/r_a & 1/r_b & 1/r_c \\ 1/r_a & 1/R_{2,a} & 1/l & 1/2l \\ 1/r_b & 1/l & 1/R_{2,b} & 1/l \\ 1/r_c & 1/2l & 1/l & 1/R_{2,c} \end{bmatrix}}_{[C_M]^{-1}} \begin{bmatrix} q_1 \\ q_a \\ q_b \\ q_c \end{bmatrix} \tag{5}$$

The potentials $\phi_1$ and $\phi_2$ are the potentials of the 2 vehicles, while $q_1$ is the charge on the spherical vehicle 1, while $q_a$, $q_b$ and $q_c$ are the charges of the spheres representing the cylinder. By inverting $[C_M]^{-1}$, the charge on each sphere is determined

at any time. The charge redistribution and interaction with the space environment is assumed to be orders of magnitude faster than the spacecraft motion. As an example, with charge control the response time is on the order of milliseconds in GEO [32, 33]. The total electrostatic force and torque about the center of the cylinder are then given by the summations

$$\boldsymbol{F}_2 = k_c q_1 \sum_{i=a}^{c} \frac{q_i}{{r_i}^3} \boldsymbol{r}_i \tag{6}$$

$$\boldsymbol{L}_2 = k_c q_1 \sum_{i=a}^{c} \frac{q_i}{{r_i}^3} \boldsymbol{r}_{2,i} \times \boldsymbol{r}_i \tag{7}$$

The cylinder center is also assumed to be the cylinder center-of-mass. In Eq. 7, only the outer two spheres contribute to the total torque on the spacecraft, while the MSM center sphere cannot produce a torque, only a force. By considering the effective moment arms at each sphere, this summation can be simplified into the following torque magnitude expression:

$$L_2 = k_c q_1(d,\theta) l d \sin\theta \left( \frac{q_c(d,\theta)}{r_c^3(d,\theta)} - \frac{q_a(d,\theta)}{r_a^3(d,\theta)} \right) \tag{8}$$

This expression is still rather complex with the implicit dependency of the charges on the relative position states $d$ and $\theta$. The following section thus seeks simplified analytical expressions about nominal relative position states.

A free body diagram of the system is shown in Fig. 2. Note that, because the individual forces on sphere 1 are equal and opposite to those on the spheres in the cylinder,

$$\boldsymbol{F}_1 = -\boldsymbol{F}_2 \tag{9}$$

Body 1 does not experience a torque, but together with the force and torque on the cylinder, the translational and rotational momentum due to electrostatic interactions is conserved. Assuming the cylinder is not capable of active translational control, a

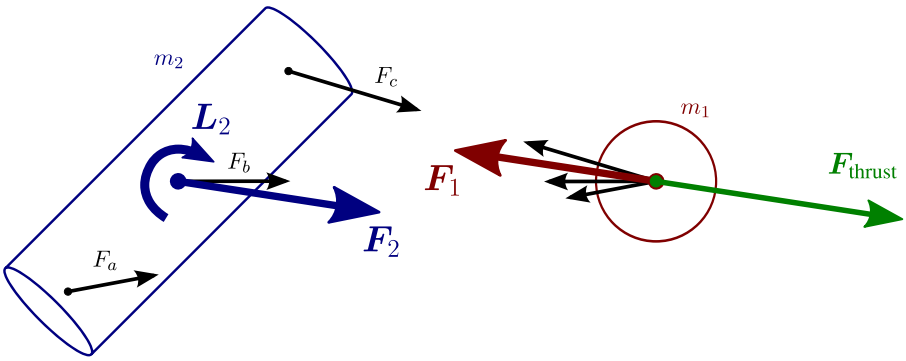


**Fig. 2** Free body diagram for MSM cylinder-sphere system

thrusting force on body 1 is necessary to maintain a constant relative position within the system:

$$\boldsymbol{F}_{\text{thrust}} = -\boldsymbol{F}_1 \left(1 + \frac{m_1}{m_2}\right) \tag{10}$$

This thrusting force provides the energy necessary to adjust the attitude of the cylinder. Though the system continually moves in space, the craft are fixed relative to each other and can be assumed stationary for the control development.

For this manuscript's simulations, system parameters are chosen as in Table 1. As in Reference [20], the cylinder is 3m long by 1m in diameter, while $R_1 = 0.5$m. A nonlinear fit is performed to determine the optimal sphere parameters that match a set of accepted numerically determined force and torque values at various orientations and separation distances.

## Analytic Torque Representation

Unfortunately, Eq. 7 does not produce a simple analytic expression for the cylinder torque in terms of the voltages and cylinder attitude, because of the 4×4 matrix inversion necessary to find the charge on each sphere. By a combination of analytic software manipulation of the equations, and numerical fitting schemes, several simplifications can be made.

Assume first that both bodies have the same potential magnitude $\phi_2 = |\phi_1|$. Body 1 has a potential $\phi_1$ which can have either sign. The tumbling body 2 is assumed to have $\phi_2 \geq 0$ without loss of generality. If this condition is satisfied, the expression for the torque $L = L_2$ can be separated into dependencies on the control voltage $\phi_1$ and cylinder rotation angle $\theta$:

$$L = \gamma f(\phi) g(\theta) \tag{11}$$

If this separation of potential $\phi_1$ and orientation $\theta$ is not warranted by looking at the numerical results of the electrostatic field modeling, then the process of extracting the required control potential from the charged attitude feedback is significantly complicated. For the cylinder shape, this separation is justified by restricting the potentials to $\phi_2 = |\phi_1|$ and assuming the cylinder is symmetric.

**Table 1** Parameters for cylinder de-spin system

| Parameter | Value | Units | Description |
|---|---|---|---|
| $d$ | 15 | m | Object center-to-center separation |
| $l$ | 1.1569 | m | MSM Parameters |
| $R_{2,a}$, $R_{2,c}$ | 0.5909 | m | MSM Parameters |
| $R_{2,b}$ | 0.6512 | m | MSM Parameters |

Figure 3 shows the torque solution $L$ as developed in Eq. 7 in terms of the independent control voltages $\phi_1$ and cylinder rotation angle $\theta$. The separation distance is shown for $d = 2.5$ m and $d = 15$ m. The voltage dependency function is set to:

$$f(\phi_1) = \phi_1|\phi_1| \tag{12}$$

The orientation angle dependency shows some complicated trends for close proximity craft (Fig. 3a), resulting from a complicated angle and voltage dependency due to induced charge effects. For the desired separation distance $d = 15$m, however, it can be fit very well to the function

$$g(\theta) = \sin 2\theta \tag{13}$$

as shown in Fig. 3b. In this setup, the slender symmetry cylinder axis is assumed to be aligned with the inter-spacecraft center of mass axis when $\theta = 0^{\text{o}}$. The optimized coefficient $\gamma$ is found to be $\gamma = 2.234 \times 10^{-14}$, a positive value for this zero $\theta$ angle reference assumption, and resulting in a very accurate fit with $R^2 = 0.9998$. Note that if the cylinder were oblate, rather than prolate, the sign of $\gamma$ could switch.

## Constant Potential Equilibrium Attitudes

For the following developments, the function $f$ in Eq. 11 must be invertible and posses the property $f(\phi)\phi \geq 0$. These requirements are satisfied by the relation in Eq. 12. The one-dimensional rotational equation of motion is given by

$$I\ddot{\theta} - \gamma f(\phi_1)g(\theta) = 0 \tag{14}$$

The relative position vectors are held fixed in this study. An inertial control solution is assumed to be present on body 1 which maintains a constant separation distance while controlling the tumble rate of body 2. This is a good assumption for the electrostatic tug case where inertial thrusters on the tug craft are used to maintain a fixed relative position.

To evaluate the equilibrium orientations, and study the associated local stability, let $\theta_{e,i}$ be the set of orientation angles such that $g(\theta_{e,i}) = 0$. Note that the zero reference orientation is chosen such that $\theta_{e,1} = 0^{\text{o}}$. The constant $\gamma$ can be either positive or

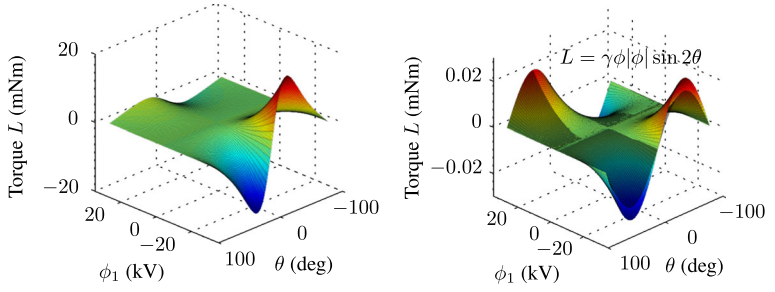


(a) $d = 2.5$ m (b) $d = 15$ m

**Fig. 3** Torques on cylinder by MSM at two different separation distances with an analytic fit for $d = 15$ m

negative, depending on the three-dimensional shape of the tumbling object. Let a small departure angle $\Delta\theta$ be defined as

$$\Delta\theta = \theta - \theta_{e,i} \tag{15}$$

The linearized rotational equation of motion about an equilibrium orientation $\theta_{e,i}$ is then given by

$$I\,\Delta\ddot{\theta} + k\Delta\theta = 0 \tag{16}$$

where the local stiffness $k$ is defined as:

$$k = -\gamma f(\phi_1)\frac{\partial g}{\partial \theta}\Big|_{\theta=\theta_{e,i}} \tag{17}$$

Assume that $f(\phi)$ and $g(\theta)$ are given by the fit outlined in Eqs. 12 and 13 for the 3m by 1m cylinder body. For this formulation, $\theta = 0^{\text{o}}$ corresponds to the long axis of the cylinder being in line with the line-of-sight axis. This scenario leads to $\gamma > 0$ with the chosen cylinder dimensions. The sensitivity of $g$ with respect to $\theta$ is

$$\frac{\partial g}{\partial \theta} = 2\cos(2\theta) \tag{18}$$

To study the local stability of departure motions about equilibria orientations, the sign of $k$ is investigated for different scenarios illustrated in Fig. 4. The in-line equilibrium scenario shown in Fig. 4a has the cylinder long-axis nominally aligned with the line-of-sight axis.

**Case 1** Consider a repulsive scenario with $\phi_1 > 0$. The MSM results show that in this setup the constant $\gamma > 0$. The $g$ sensitivity in this case is

$$\frac{\partial g}{\partial \theta}\Big|_{\theta=0^{\text{o}}} = 2\cos(0^{\text{o}}) = 2 \tag{19}$$

Assuming a repulsive force setup with $f(\phi_1) > 0$, the local stiffness $k$ for this case is

$$k = -2\gamma f(\phi_1) < 0 \tag{20}$$

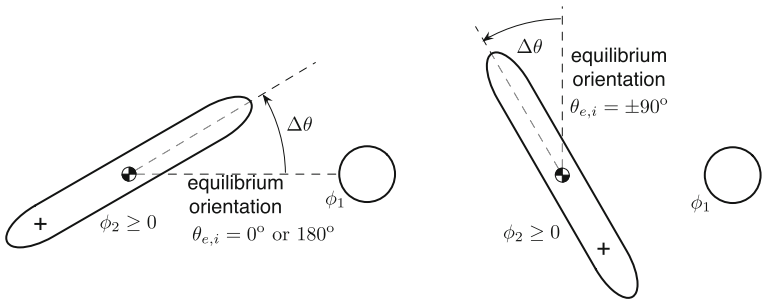


(a) In-Line Equilibrium Configuration (b) Cross-Track Equilibrium Configuration

**Fig. 4** Departure angle illustration with respect to in-line and cross-track equilibriums

indicating an unstable equilibrium. Studying Fig. 4a, this instability can be understood because the near-end of the cylinder experiences a stronger repulsion force than the far end, and thus the resulting electrostatic torque will cause a destabilizing effect.

**Case 2** Keeping the nominal orientation shown in Fig. 4a, next assumes that the sphere potential is negative with $\phi_1 < 0$, and an attractive electrostatic force is present. Because $f(\phi_1) < 0$ now, the local stiffness is

$$k = -2\gamma f(\phi_1) > 0 \tag{21}$$

indicating a locally stable equilibrium. Due to symmetry of the tall cylinder, considering $\theta_{e,i} = 180^{\text{o}}$ yields the same result.

**Case 3** Next, consider the equilibria shown in Fig. 4b where the cylinder long axis is orthogonal to the line-of-sight axis. Here the $g$ sensitivity is

$$\frac{\partial g}{\partial \theta}\Big|_{\theta=\pm 90^{\text{o}}} = 2\cos(\pm 180^{\text{o}}) = -2 \tag{22}$$

Assuming a repulsive force configuration with $f(\phi_1) > 0$, the local stiffness is

$$k = 2\gamma f(\phi_1) > 0 \tag{23}$$

Thus, if bodies 1 and 2 are electrostatically pushing on each other, then $\theta_{e,i} = \pm 90^{\text{o}}$ are locally stable orientations.

**Case 4** Finally, assuming the Cross-Track scenario in Fig. 4b and a pulling configuration with $f(\phi_1) < 0$, the local stiffness is

$$k = 2\gamma f(\phi_1) < 0 \tag{24}$$

indicating that such an orientation is locally unstable.

## Rate Control with Zero Nominal Potential

### Feedback Control Development

The following feedback control developments all have the common goal of arresting the tumbling of body 2. Both bodies are assumed to be in deep space, absent from gravitational torques of celestial bodies. In all cases the relative position between the two bodies is held fixed. This is assumed to be achieved with an inertial thruster control strategy on body 1, as is described in Reference [25]. First, the scenario is investigated where the nominal spacecraft potential is zero. Thus, when the tumbling motion has been arrested, no electrostatic pulling or tugging should be present. The inertial thrust to maintain a fixed separation distance will also go to zero as the tumbling ceases.

The potentials $\phi_1$ and $\phi_2$ are controlled in a coordinated manner assuming the potential magnitudes are always equal. This allows for the electrostatic torque model of the form given in Eq. 11. Further, for the electrostatic tug application this equal

potential condition will result in the largest electrostatic tractor force. The control development assumes that the tumbling angle $\theta$ and rate $\dot{\theta}$ are measured, and that the spacecraft 1 potential $\phi_1$ is the control variable.

Let $\alpha > 0$ be a constant rate feedback gain. The function $h$ is chosen such that

$$h(x)x > 0 \quad \text{if } x \neq 0 \tag{25}$$

forms a positive definite expression. Then, the following tumble rate feedback control $f(\phi_1)$ is proposed:

$$f(\phi_1) = -\frac{\text{sgn}(g(\theta))}{\gamma} h(\alpha\dot{\theta}) \tag{26}$$

Depending on the final implementation of this control, note that the sgn() function can cause chatter issues if measurement noise is considered. Without loss of the following stability claims, this sgn() could be replaced with a smoothed sigmoid function. The sgn() is retained here as it leads to a simpler analysis. Further, implementing relatively fast changes in potentials is practical, as active charging in space has a response time of a fraction of a second [34]. Because the function $f$ is invertible, (26) can be inverted to yield the required potential $\phi_1$ of body 1. The potential $\phi_2$ of body 2 is then controlled to be $\phi_2 = |\phi_1|$. Note that if the approximate electrostatic torque did not have the separation of potential and relative orientation, as formulated in Eq. 11, then the potential feedback control development becomes significantly more complex. In particular, due to the coupling between orientation and potential, it may not be possible to extract the control potential $\phi_1$ analytically, in which case numerical solvers are required to determine the control. As is, the potential control development only requires $f$ and $g$ to satisfy some simple conditions to guarantee stability. In particular, the $g(\theta)$ function approximation could be further refined, without having to develop a new rate feedback control strategy.

The function $h$ is introduced to yield a general feedback control whose performance can be modified. For example, the simple linear function $h(\alpha\dot{\theta}) = \alpha\dot{\theta}$ can be used. However, the resulting control potentials will grow large if large initial tumble rates $\dot{\theta}$ are considered. If the available potentials are bounded to be less than $\phi_{\max}$, then the following $h$ function will smoothly limit or saturate the control without impacting the following stability discussion:

$$h(\alpha\dot{\theta}) = f(\phi_{\max})\gamma \frac{\arctan(\alpha\dot{\theta})}{\pi/2} \tag{27}$$

As the tumble rate $\dot{\theta} \to \infty$, then $\arctan(\alpha\dot{\theta}) \to \pi/2$, and

$$\lim_{\dot{\theta}\to\infty} h(\alpha\dot{\theta}) = f(\phi_{\max})\gamma \tag{28}$$

Thus, the control effort for large rates $\dot{\theta}$ is smoothly limited with this $h$ function in Eq. 27 by

$$\lim_{\dot{\theta}\to\infty} f(\phi_1) = \begin{cases} -f(\phi_{\max}) & \text{if } g(\theta) > 0 \\ 0 & \text{if } g(\theta) = 0 \\ f(\phi_{\max}) & \text{if } g(\theta) < 0 \end{cases} \tag{29}$$

### Stability Analysis

To investigate the stability of this potential feedback control law in Eq. 26, the rotational kinetic energy is used as a globally positive definite Lyapunov candidate function $V$.

$$V(\dot{\theta}) = \frac{I}{2}\dot{\theta}^2 \tag{30}$$

The presented control only aims to arrest the spin rate, and does not seek to achieve a particular relative orientation angle $\theta$. Taking the time derivative of $V$, and substituting the equations of motion $I\ddot{\theta} = L$ leads to

$$\dot{V} = L\dot{\theta} = \gamma f(\phi_1) g(\theta)\dot{\theta} \tag{31}$$

Substituting in the control expression in Eq. 26 and simplifying leads to

$$\dot{V} = -|g(\theta)|h(\alpha\dot{\theta})\dot{\theta} \leq 0 \tag{32}$$

This $\dot{V}$ expression is globally negative semi-definite as $h(\alpha\dot{\theta})\dot{\theta}$ is a positive definite expression. Note that $\dot{V}$ can become zero at the equilibrium orientations $\theta_{e_i}$ where $g(\theta_{e,i}) = 0$. Thus, Eq. 32 guarantees globally stable tumbling rate closed loop dynamics.

To study convergence, LaSalle's invariance principle is employed [35]. The Lyapunov rate $\dot{V}$ is zero either if the rate $\dot{\theta}$ is zero and the control goal is achieved, or if $g(\theta) = 0$. The later condition forces $\dot{V}$ to zero regardless if $\dot{\theta}$ is zero. Assuming there are orientations such that $g(\theta) \neq 0$ (i.e. the second body is not a sphere) it is not possible for the condition $g(\theta) = 0$ to remain true unless $\dot{\theta} = 0$ as well. Thus, the largest invariant set where $\dot{V}$ vanishes is $(\theta, \dot{\theta}) = \{\dot{\theta} = 0\}$. As a result, this potential feedback control achieves global convergence in driving the rates to zero. The final orientation, however, is arbitrary with this control. This is in contrast to the control presented next, where nominal tugging or pushing is present.

### Control with only Positive or Negative Potentials

The potential control in Eq. 26 assumes that both positive and negative potentials can be created on body 1. This could be implemented by having both vehicles use their own charge emission devices to control their potentials. However, if one of the bodies is charged using touchless charge transfer, i.e. charge beaming, then it is simpler to implement only attractive electrostatic forces. For example, if vehicle 1 is charged negatively using an ion emitter, and the ion emission is aimed at the second vehicle, the latter will charge positively and create an attractive electrostatic force. Such indirect charging is of great interest to electrostatic geostationary debris removal [24, 25, 36]. The following simple modification of the potential control in Eq. 26 provides the ability to only use attractive or repulsive electrostatic forces to control the spin rate.

To allow for mono-polarity charges on the control vehicle 1, the control gains $\alpha$ are set to zero if the potential control in Eq. 26 requires an undesired sign. For

example, if only non-positive potentials $\phi_1$ are desired, the control is chosen through the logic:

$$\phi_1 = \begin{cases} f^{-1} & \text{if } f \leq 0 \\ 0 & \text{if } f > 0 \end{cases} \tag{33}$$

This simple modification doesn't change the global stability argument as $\dot{V}$ remains negative semi-definite. Similarly, the largest invariant set where $\dot{V}$ vanishes is the set where $\dot{\theta}$ is zero, because $\dot{\theta}$ remains constant and non-zero as body 2 rotates through the region where the control is inactive, and thus it cannot remain there. Thus, convergence is unchanged as well. While this modification doesn't impact the earlier stability arguments, naturally, it will impact the performance and cause the control to take about twice as long to despin the second body.

## Rate Control with Nominal Electrostatic Tugging or Pushing

Electrostatic forces have been proposed to reorbit large geosynchronous debris objects to disposal orbits [24, 25, 36]. Because the large, bus-sized GEO debris can be tumbling at 10s of degrees per second, not having to mechanically touch the debris is a significant advantage. While the pulling configuration with a nominal attractive electrostatic force is the preferred configuration [37], pushing configurations are also feasible. The earlier rate-control is modified such that the nominal potential $\phi$ is non-zero, allowing for continuous pulling ($\phi_1\phi_2 < 0$) or pushing ($\phi_1\phi_2 > 0$).

### Feedback Control Development

To investigate detumbling a rigid body while also electrostatically pulling or pushing this object, the following Lyapunov candidate function is considered:

$$V(\theta, \dot{\theta}) = \frac{I}{2}\dot{\theta}^2 + \beta \int_0^{\theta} g(x)\mathrm{d}x \tag{34}$$

where $\beta > 0$ is a feedforward constant of the resulting control. The integral term of this $V$ expression is locally positive definite if a reference orientation $\theta = 0$ is chosen such that

$$\frac{\partial g(\theta)}{\partial \theta}\Big|_{\theta=0} > 0 \tag{35}$$

This condition has an impact on the final convergence of the rate control. Note that this Lyapunov function depends both on the rate and orientation variables, as the pushing/pulling condition will have an impact on the final orientation of the second body.

Taking the time derivative of Eq. 34, and substituting Eqs. 11 and 14, yields the following Lyapunov rate expression:

$$\dot{V}(\theta, \dot{\theta}) = (\gamma f(\phi_1) g(\theta) + \beta g(\theta))\,\dot{\theta} \tag{36}$$

Let the new potential control expression be:

$$f(\phi_1) = \underbrace{-\frac{\beta}{\gamma}}_{f_0} - \frac{\text{sgn}(g(\theta))}{\gamma} h(\alpha\dot{\theta}) \tag{37}$$

where $f_0$ represents the feedforward component of the potential control. Given a nominal potential $\phi_{\text{nom}}$, the positive feedforward gain $\beta$ is chosen to be

$$\beta = -f(\phi_{\text{nom}})\gamma \tag{38}$$

such that the appropriate $f_0$ results. Note that $\beta > 0$ requires that $\phi_{\text{nom}}$ and $\gamma$ have the opposite sign.

Substituting Eq. 37 into Eq. 36 yields the reduced Lyapunov rate expression:

$$\dot{V} = \left(-\gamma\frac{\beta}{\gamma}g(\theta) - \gamma\frac{\text{sgn}(g(\theta))}{\gamma}h(\alpha\dot{\theta})g(\theta) + \beta g(\theta)\right)\dot{\theta} \tag{39}$$

$$= -|g(\theta)|h(\alpha\dot{\theta})\dot{\theta} \leq 0 \tag{40}$$

Note that the integral term in the Lyapunov expression causes a cancellation with the feedforward potential term, resulting in a negative semi-definite $\dot{V}$ expression. The feedforward/feedback control in Eq. 37 is thus at least locally stable. This is interesting considering $V$ depends on both $\theta$ and $\dot{\theta}$, as it implies that the configuration is also stable about the reference orientation.

From the earlier linear stability discussion with constant potentials, the two stable configurations while either pulling (Case 2) or pushing (Case 3) are illustrated in Fig. 5. For the pulling configuration $\gamma > 0$, which leads to a feedforward term of

$$f_0 = -\frac{\beta}{\gamma} < 0 \tag{41}$$

indicating that the nominal spacecraft potential must be negative, creating an attractive force, for this orientation to be stable. In contrast, if $\theta$ is measured from the 90°

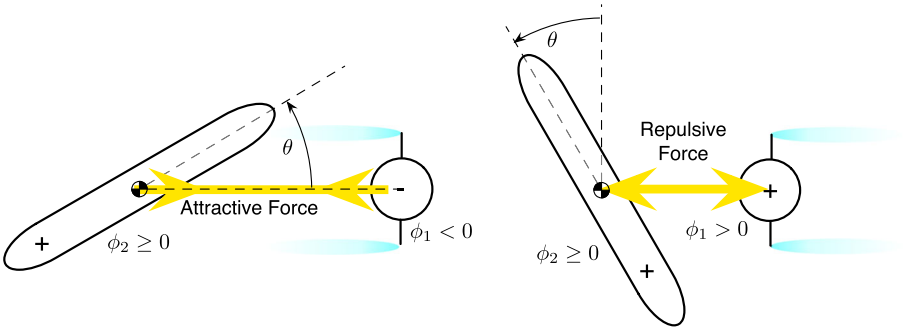


(a) Pulling Configuration with $\gamma > 0$ (b) Pushing Configuration with $\gamma < 0$

**Fig. 5** Illustration of pulling and pushing configurations

cross-axis as indicated in Fig. 5b, then $\gamma < 0$ and the feedforward control component must be

$$f_0 = -\frac{\beta}{\gamma} > 0 \tag{42}$$

This indicates the nominal potential $\phi_1$ must be positive, creating a repulsive force.

Next, the convergence of this feedback/feedforward control is investigated. Without loss of generality, $\gamma > 0$ is assumed. As before, $\dot{V}$ vanished if either $\dot{\theta} =$ or $g(\theta) = 0$. The earlier control resulted in $\dot{\theta} \to 0$ in all cases, but the final orientation was arbitrary depending on the initial conditions. With the feedforward component of the control the attitude will converge to discrete orientations. The closed loop dynamics using the control in Eq. 37 is

$$I\ddot{\theta} + \beta g(\theta) + |g(\theta)|h(\alpha\dot{\theta}) = 0 \tag{43}$$

Again, it is not possible for $g(\theta) = 0$ to remain true if $\dot{\theta} \neq 0$. However, can $g(\theta)$ remain non-zero if $\dot{\theta}$ is zero? Setting the rate to zero in Eq. 43 yields

$$I\ddot{\theta} = -\beta g(\theta) \tag{44}$$

This indicates that $\ddot{\theta}$ cannot remain zero unless both $\dot{\theta} = 0$ and $g(\theta) = 0$. Thus, the largest invariant set where $\dot{V}$ vanishes is $\theta = \theta_{e,i}$ and $\dot{\theta} = 0$. In contrast to the rate-only feedback, this feedforward/feedback control has the rate converge to zero, and the orientation converge to a torque equilibrium orientation. For the torque shape function $g(\theta) = \sin(2\theta)$ two of these equilibria were unstable, and two were stable. If small perturbations are considered, the second body would not be able to remain at an unstable equilibrium, but will eventually converge to a stable equilibrium.

To study this stability behavior, consider the Lyapunov surface illustration in Fig. 6 where the function $g(\theta) = \sin(2\theta)$ is used with unit inertia and unit feedforward gain. The largest Lyapunov level about the origin is highlighted for convenience. For initial conditions outside this level set, it is possible for the second body to stabilize about the stable equilibrium $\theta_e = 180^o$. This illustrates that the control in Eq. 37 is indeed only locally stable. However, if the control objective is changed to arrest

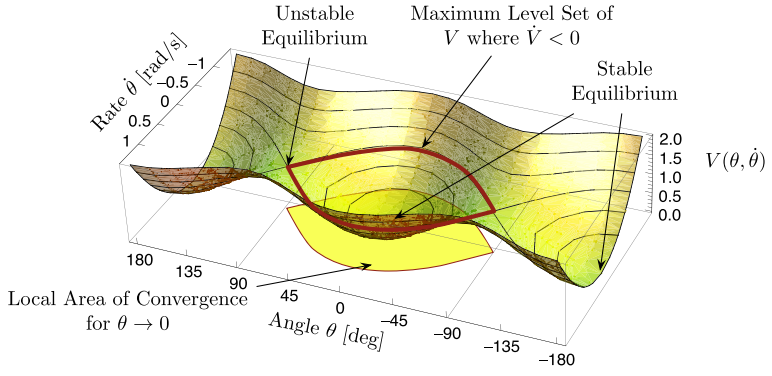


**Fig. 6** Illustration of Lyapunov function and level sets for unit inertia $I$ and gain $\beta$

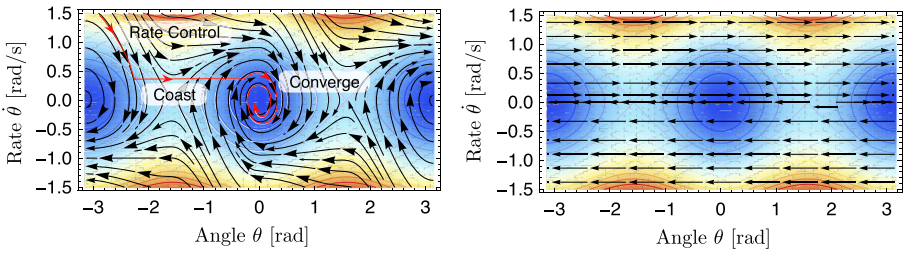


(a) Active Control Scenario (b) No Control Scenario

**Fig. 7** State space flow illustration in relation to Lyapunov level sets

the rate, and align the body with either $\theta = 0^o$ or $180^o$, then the control is globally asymptotically stabilizing. However, no control is present to chose which of these two orientations the body will converge to.

The contour plot in Fig. 7a illustrates the closed loop trajectories if the control in Eq. 37 is active. Depending on the initial conditions, the trajectories can either converge to the stable equilibria at 0 or 180 degrees, or approach the $\pm 90$ degree unstable equilibria. If it is important that the tumbling body settle with a particular end (either $\theta = 0^o$ or $180^o$), then the following strategy can be employed. Figure 7b illustrates the state trajectories if no control is present, and the second body continues to tumble at a constant rate. The horizontal flow lines can be exploited to move the states of the tumbling body into a preferred zone where convergence to a particular equilibrium orientation is guaranteed. This process is highlighted in red in Fig. 7a. The rate control is first employed until the rates are small enough to guarantee convergence to an equilibrium. If this is not the desired equilibrium, turning off the potential control will allow the body to tumble onward. As the state trajectory enters the local area of convergence of the desire equilibrium orientation, the feedback control is re-engaged to arrest the final rates and drive $\theta \to \theta_e$.

**Table 2** Parameters for cylinder tug/de-spin simulation

| Parameter | Value | Units | Description |
|---|---|---|---|
| $\rho$ | 100 | kg/m$^2$ | Object densities |
| $m_1$ | 52.4 | kg | Sphere mass |
| $m_2$ | 235.6 | kg | Cylinder mass |
| $I_1$ | 191.4 | kg·m$^2$ | Cylinder transverse moment of inertia |
| $\omega_0$ | 2 | deg/sec | Initial cylinder rotation rate |
| $\alpha$ | $5\times10^4$ | – | Gain in $h$ function |
| $\phi_{\text{nom}}$ | -15 | kV | Nominal voltage in $f$ function |
| $\phi_{\text{max}}$ | 20 | kV | Max voltage in $h$ function |
| | 1 | Hz | Simulated control and sensor frequency |

## Numerical Simulation

A numerical simulation is performed to verify the control laws presented above. Specifically, rate control with a nominal electrostatic tug is implemented. Here a rotating cylinder in deep space is de-spun while it is tugged along by the neighboring spherical craft. The voltage on both objects is affected by voltage control devices on the spherical craft. Note that no sensors errors, or voltage control errors, are modeled in this study. This allows for a better illustration of the idealized attitude control performance. How to control the potential on both bodies is a challenging tasks that warrants its own investigation, coupled with the options of charge/potential sensors. The simulation is performed with full six degrees of freedom, and a PID thruster

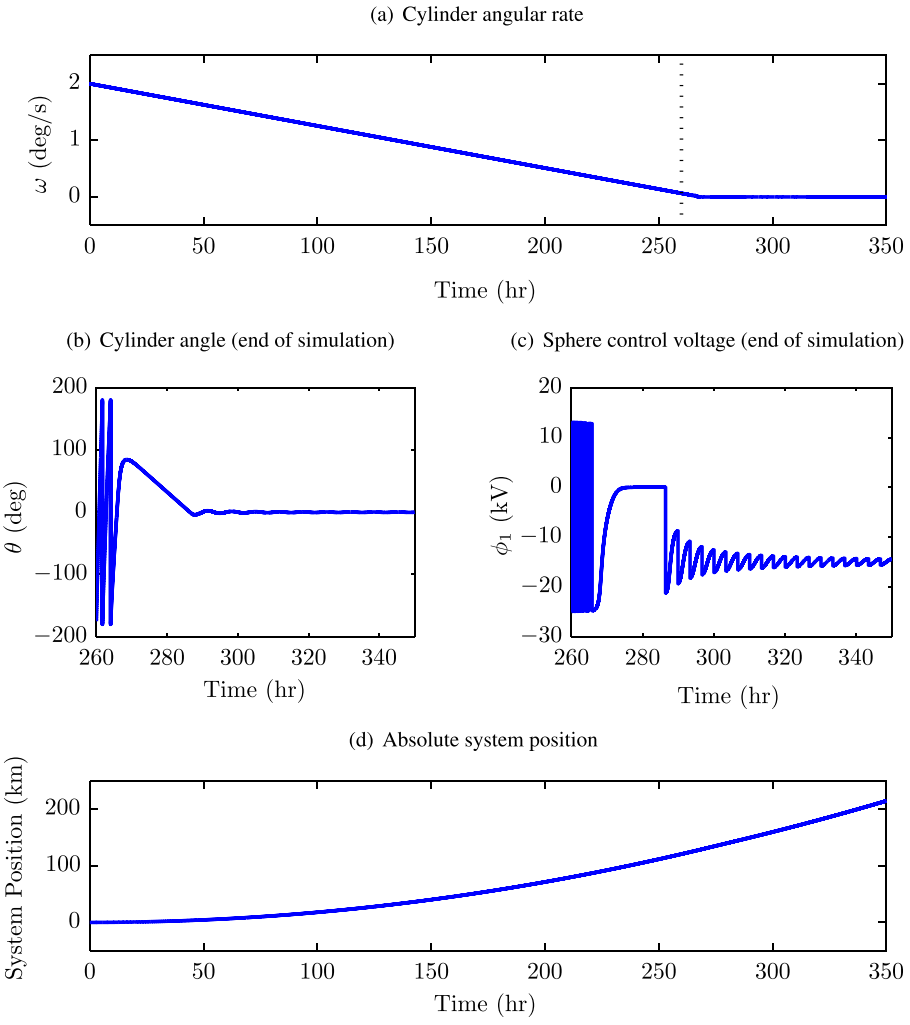


**Fig. 8** Cylinder tug and de-spin simulation using Coulomb charge control

control is implemented on the spherical craft to ensure the desired separation is maintained. Table 1 shows the MSM cylinder parameters and nominal separation distance, while Table 2 provides the remaining necessary system and control parameters. The pulling sphere (for example the electrostatic tug) is of rather small size of $R_1 = 0.5$ meters. Figure 8 displays the simulation results. Even this small tug dimensions can already exert a significant electrostatic torque.

The potential control expression $f(\phi_1)$ in Eq. 37 is used, while Eq. 27 defines the function $h$. Because Eq. 37 contains a nominal and de-spin term, the true voltage limits during the de-spin procedure are:

$$\phi_{\text{lower}} = -\sqrt{{\phi_{\text{nom}}}^2 + {\phi_{\text{max}}}^2} \tag{45}$$

$$\phi_{\text{upper}} = +\sqrt{-{\phi_{\text{nom}}}^2 + {\phi_{\text{max}}}^2} \tag{46}$$

Once the cylinder stops making full rotations, the nominal control voltage is indeed $\phi_{\text{nom}}$ and this behavior is clearly visible in Fig. 8c.

From Fig. 8a and b it is clear that the cylinder stops spinning after roughly 275 hours or just over 11 days, during which time 2798 full rotations have been completed. Although 2 deg/sec is not an especially fast initial spin rate, a de-spin by electrostatic actuation in this time is impressive considering the momentum of the cylinder and separation distance between the craft. Figure 8d shows that the system has been displaced by more than 200 km during the de-spin, which represents a considerable electrostatic tug.

## Conclusion

The relative attitude control using spacecraft potential control is investigated for a one-dimensional rotation scenario. If the vehicles are within 3-4 craft radii, the electrostatic torques can have a significant impact on the rotational motion. For example, it is envisioned that electrostatic torques could be used to detumble a large geostationary debris object. Using the multi-sphere method, a simplified electrostatic torque model is employed to numerically study the charged relative attitude motion. For a cylinder-sphere scenario, a suitable reduced order torque expression is used for feedback control development. The potential control is analytically proven to bring the tumbling objects attitude rate to zero, but the final orientation is arbitrary and uncontrolled. If the nominal spacecraft potential is nonzero, then a potential feedback control is shown to cause the object to settle to a stable torque equilibrium orientation while the tractor force is maintained. Future work will investigate the torques between more complex shapes, as well as expand the control to encompass general three-dimensional rotational motion. If the body is fully conducting and has a symmetry axis, then rotations about this symmetry axis are not directly controllable with this method. In this case the complex gyroscopic coupling must be investigated to see if this spin can be indirectly controlled. Further, the robustness of this attitude control strategy with respect to attitude sensor and voltage servo control errors should be considered.

**Acknowledgments** We would like to thank Erik Hogan for the helpful discussion on the analytical convergence results with electrostatic torques.

## References

1. Cover, J.H., Knauer, W., Maurer, H.A.: Lightweight reflecting structures utilizing electrostatic inflation. US Patent **3**, 546,706 (1966)
2. King, L.B., Parker, G.G., Deshmukh, S., Chong, J.-H.: Study of interspacecraft coulomb forces and implications for formation flying. AIAA J. Propuls. Power **19**, 497–505 (2003)
3. Berryman, J., Schaub, H.: Analytical charge analysis for 2- and 3-craft coulomb formations. AIAA J. Guid. Control. Dyn. **30**, 1701–1710 (2007)
4. Schaub, H., Hall, C., Berryman, J.: Necessary conditions for circularly-restricted static coulomb formations. J. Astronaut. Sci. **54**, 525–541 (2006)
5. Berryman, J., Schaub, H.: Static equilibrium configurations in GEO coulomb spacecraft formations, Advances in Astronautical Sciences, vol. 120, American Astronautical Society, 2005, pp. 51–68. Paper No. AAS 05–104
6. Natarajan, A., Schaub, H.: Linear dynamics and stability analysis of a coulomb tether formation. AIAA J. Guid. Control. Dyn. **29**, 831–839 (2006)
7. Natarajan, A., Schaub, H.: Orbit-nadir aligned coulomb tether reconfiguration analysis. J. Astronaut. Sci. **56**, 573–592 (2008)
8. Natarajan, A., Schaub, H., Parker, G.G.: Reconfiguration of a nadir-pointing 2-craft coulomb tether. J. Br. Interplanet. Soc. **60**, 209–218 (2007)
9. Natarajan, A., Schaub, H.: Hybrid control of orbit normal and along-track two-craft coulomb tethers. Aerosp. Sci. Technol. **13**, 183–191 (2009)
10. Izzo, D., Pettazzi, L.: Autonomous and distributed motion planning for satellite swarm. J. Guid. Control Dyn. **30**(2), 449–459 (2007)
11. Pettazzi, L., Krüger, H., Theil, S., Izzo, D.: Electrostatic forces for satellite swarm navigation and reconfiguration. In: 2nd ACT Workshop on Innovative Concepts, ESTEC (2008)
12. Izzo, D., Pettazzi, L.: Self-assembly of large structures in space using intersatellite Coulomb forces. In: 57th International Astronautical Congress, Valencia, Spain, October 2006. Paper IAC-06-C3.4/D3.4.07
13. Pettazzi, L., Izzo, D., Theil, S.: Swarm navigation and reconfiguration using electrostatic forces. In: 7th International Conference on Dynamics and Control of Systems and Structures in Space, Greenwich, London, England, pp. 257–267 (2006)
14. Peck, M.A.: Prospects and challenges for lorentz-augmented orbits. In: AIAA Guidance, Navigation and Control Conference, San Francisco, CA, August 15–18 2005. Paper No. AIAA 2005-5995
15. Peck, M.A., Streetman, B., Saaj, C.M., Lappas, V.: Spacecraft formation flying using lorentz forces. J. Br. Interplanet. Soc. **60**, 263–267 (2007)
16. Gangestad, J., Pollock, G., Longuski, J.: Lagrange's planetary equations for the motion of electrostatically charged spacecraft. Celest. Mech. Dyn. Astron. **108**, 125–145 (2010). doi:10.1007/s10569-010-9297-z
17. Schaub, H., Parker, G.G., King, L.B.: Challenges and prospect of coulomb spacecraft formation control. J. Astronaut. Sci. **52**, 169–193 (2004)
18. Seubert, C.R., Schaub, H.: Closed-loop one-dimensional charged relative motion experiments simululating constrained orbital motion. AIAA J. Guid. Control. Dyn., 1856–1865 (2009). doi:10.2514/1.48274
19. Seubert, C.R., Schaub, H.: Electrostatic force model for terrestrial experiments on the coulomb testbed. In: 61st International Astronautical Congress, Prague, CZ, International Astronautical Federation, Sept. 2010. Paper IAC-10.C1.1.9
20. Stevenson, D., Schaub, H.: Multi sphere modeling for electrostatic forces on three-dimensional spacecraft shapes. In: AAS/AIAA Spaceflight Mechanics Meeting, Charleston, South Carolina, Jan. 29 – Feb. 2 2012. Paper AAS 12-106
21. Stevenson, D.: Optimization of sphere population for electrostatic multi sphere model. In: 12th Spacecraft Charging Technology Conference, Kitakyushu, Japan, May 14–18 (2012)
22. Smythe, W.R.: Static and dynamic electricity. McGraw–Hill, 3rd ed. (1968)

23. Sliško, J., Brito-Orta, R.A.: On approximate formulas for the electrostatic force between two conducting spheres. Am. J. Phys. **66**(4), 352–355 (1998)
24. Schaub, H., Moorer, D.F.: Geosynchronous large debris reorbiter: challenges and prospects. In: AAS Kyle T. Alfriend Astrodynamics Symposium, Monterey, CA, May 17–19 2010. Paper No. AAS 10-311
25. Hogan, E., H. Schaub: Relative motion control for two-spacecraft electrostatic orbit corrections. In: AAS/AIAA Spaceflight Mechanics Meeting, Girdwood, Alaska, July 31 – August 4 2011. Paper AAS 11–466
26. Denton, M.H., Thomsen, M.F., Korth, H., Lynch, S., Zhang, J.C., Liemohn, M.W.: Bulk plasma properties at geosynchronous orbit. J. Geophys. Res. **110**, 07 (2005)
27. Mullen, E.G., Gussenhoven, M.S., Hardy, D.A., Aggson, T.A., Ledley, B.G.: SCATHA survey of high-voltage spacecraft charging in sunlight. J. Geophys. Res. **91**(A2), 1474–1490 (1986). doi:10.1029/JA091iA02p01474
28. Gibson, W.C.: The method of moments in electromagnetics. Chapman & Hall, November 28 (2007)
29. Sadiku, M.N.: Monte carlo methods for electromagnetics. CRC Press (2009)
30. Jasper, L.E.Z., Schaub, H.: Effective sphere modeling for electrostatic forces on a three-dimensional spacecraft shape. In: AAS/AIAA Spaceflight Mechanics Meeting, Girdwood, Alaska, July 31 – August, 4 (2011)
31. Stiles, L.A., Seubert, C.R., Schaub, H.: Effective coulomb force modeling in a space environment. In: AAS Spaceflight Mechanics Meeting, Charleston, South Carolina, Jan. 29 – Feb. 2 2012. Paper AAS 12
32. Fennell, J.F., Koons, H.C., Leung, M., Mizera, P.: A review of SCATHA satellite results: Charging and discharging, 1983.,1983, pp. 3–11
33. Shuman, B., Cohen, H., Hyman, J., Robson, R., Santoru, J., Williamson, W.: Automatic charge control system for geosynchronous satellites. J. Electrost. **20**(1), 141–154 (1987). doi:10.1016/0304-3886(87)90091-X
34. Craven, P., Olsen, R., Fennell, J., Croley, D., Aggson, T.: Potential modulation on the SCATHA spacecraft. J. Spacecr. Rocket. **24**, 150–157 (1987)
35. Khalil, H.K.: Nonlinear systems. Upper saddle river, 3rd edn. Prentice-Hall, Inc., NJ (2002)
36. Hogan, E., Schaub, H.: Space debris reorbiting using electrostatic actuation. In: AAS Guidance and Control Conference, Breckenridge, CO, Feb. 3–8 2012. Paper AAS 12–016
37. Schaub, H., Jasper, L.E.Z.: Circular orbit radius control using electrostatic actuation for 2-craft configurations. In: AAS/AIAA Astrodynamics Specialist Conference, Girdwood, Alaska, July 31 – August 4 2011. Paper AAS 11–498